Society of Petroleum Engineers

SPE-195269-MS

Modeling Naturally and Hydraulically Fractured Reservoirs with Artificial Intelligence and Assisted History Matching Methods Using Physics-Based Simulators

Esmail Eltahan, Wei Yu, and Kamy Sepehrnoori, The University of Texas at Austin; Erich Kerr, EP Energy; Jijun Miao, SimTech LLC; Ray Ambrose, EP Energy

This paper was prepared for presentation at the SPE Western Regional Meeting held in San Jose, California, USA, 23-26 April 2019.

Abstract

Unconventional reservoirs typically exhibit large uncertainty in rock and fracture properties coupled with significant heterogeneity making manual history matching a challenging endeavor. Computer-assisted methods of history matching gained preference because they honor the non-uniqueness of the possible geological and fracture realizations by allowing efficient simulation sensitivities over many possible outcomes. This study integrates EDFM's fracture-modeling capabilities into an artificial intelligence-based history matching and optimization tool, to achieve more confidence and capability in simulations for production forecasting and reservoir-behavior studies.

This approach involves four main steps: (1) initializing EDFM-fracture parameters for a realization, (2) running a pre-simulation command that calls the EDFM-preprocessing engine and generates an updated model, (3) running the model on an appropriate simulator, and (4) calculating the objective function. We apply this method to perform history matching for a horizontal tight-oil well in the middle Bakken. We further repeat history matching for the same model after including a set of 1,000 randomly distributed natural fractures. In both studies, four embedded-fracture parameters are set to vary within predefined continuous ranges.

The objective is to minimize history matching error for field-recorded, bottom-hole pressure and gas production data with oil production history set as a constraint. This new method, with a more realistic fracture geometry, resulted in a better match to the field-recorded data compared to a previous study that was based on a local gird refinement model. After introducing natural fractures to the model, history-matching results displayed a trend of decreasing rock-matrix permeability and fracture conductivity compared to the original scenario without natural fractures. In this case, history matching error response was most sensitive to rock-matrix permeability followed by fracture half-length. We then made 30-year production forecast using the most optimal solutions. Accepted solutions were screened based on a cut-off value of 5% normalized history-matching error. We finally demonstrate that, even though the presence of natural fractures significantly altered the model, it did not have a major influence on long-term production.

Introduction

Improved hydraulic-fracturing treatments coupled with horizontal drilling technology made it possible for large-scale development of unconventional reservoirs over the past decade (Cipolla et al. 2010). Developing methods with the capability to evaluate reservoir performance and predict estimated ultimate recovery (EUR) has been challenging. The complexity of fracture networks, often created by multi-stage stimulation techniques, makes it difficult to track fracture geometry and to measure fracture conductivity. In addition, conventional decline rate analysis becomes difficult because of the complicated fluid flow behavior. Unlike conventional reservoirs, low-permeability (less than 0.1 md) unconventional reservoirs (URs) typically exhibit prolonged period of transient flow (Luo et al. 2011). Therefore, the industry often relies on reservoir simulation as a preferable tool for predicting unconventional reservoirs performance (Cipolla et al. 2010).

Different approaches have been proposed to simulate URs. Dual continuum models were developed by Kazemi et al. (1976) and Rossen (1977) to simulate naturally fractured reservoirs (NFRs). The same concept was extended to model URs (Ding et al. 2006; Du et al. 2010; Gong et al. 2008). In these models, fracture networks are approximated into a representative dual-porosity dual-permeability (DPDK) model. DPDK approaches generally assume uniform distribution of fractures, and hence, in many cases, fail to adequately describe fracture networks (Li et al. 2011; Moinfar et al. 2011). Cipolla et al. (2010) reported that explicit discretization of reservoir elements, such as matrix blocks and network fractures, most accurately describes URs. Although more rigorous than the available alternatives, discrete fracture models are still impractical for field scale applications because of their relatively large CPU time requirements (Yang et al. 2018).

Local grid refinement (LGR) models have been postulated to increase computational efficiency (Cipolla et al. 2010; Luo et al. 2011; Sun et al. 2014; Wantawin et al. 2017; Yu and Sepehrnoori 2018). In such models, an increasing number of grids around fractures results in increasing resolution of reservoir properties but also significantly increases computation time. Moreover, although dual-permeability, logarithmically spaced (DK-LS-LGR) models provide accurate-enough representation for reservoir modeling, they usually require fractures to align with the orientation of grid (Yang et al. 2018).

Moinfar et al. (2014) introduced a more rigorous 3D embedded discrete fracture model (EDFM), which can handle fractures with arbitrary shapes and orientations. Implementing EDFM in commercial finite-difference reservoir simulators in a non-intrusive manner provides satisfactory accuracy at a considerably lower computational cost (Xu et al. 2017a, 2017b, 2018). Furthermore, EDFM is capable of handling complex fracture geometry with the same efficiency.

Although EDFM is regarded in the literature as one of the most robust modeling methods because of its efficiency and flexibility when incorporating fractures, the EDFM integration still requires significant time to perform manual history matching and subsequent probabilistic forecasting of field cases.

Most field-scale models involve large uncertainty in geological characterization and fracture geometry. The larger the number of uncertain parameters, the more difficult it is to perform manual history matching. Manual history matching will often result in a less-than-optimal single solution disregarding the non-uniqueness of all the viable solutions. Automatic history matching has been performed using LGR models using proxy-based techniques or using time-consuming simulation-based techniques (Wantawin et al. 2017a, 2017b). In these LGR models, uncertain parameters such as fracture half-length and fracture height may only vary at a discrete level that is dependent on grid size. In contrast, using EDFM, those parameters can vary at a continuous level within a pre-defined range. For this reason, and since EDFM models are noticeably more efficient and flexible than LGR models, there is an obvious benefit for an automatic history-matching technique using EDFM.

EDFM has been applied in our in-house automatic history-matching workflow (Dachanuwattana et al. 2018a, 2018b; Yu et al. 2018; Tripoppoom et al. 2019). However, it has not been extended to work with third-party history-matching and optimization workflows where full parameterization on the natural and

induced fractures can be possible. Once we achieve such parameterization, we enable applications beyond history matching, such as sensitivity, optimization, and uncertainty-assessment studies.

In this paper, we first introduce EDFM and demonstrate its capabilities to handle complex fracture networks. We next describe our new method that enables computer-assisted history matching. This method integrates the EDFM preprocessor into the existing frameworks of the optimization software. We demonstrate the efficiency of the workflow by applying it to practical field cases. In the first case, we perform history matching to a horizontal tight-oil well in the Middle Bakken. The advantages of using EDFM over LGR models are demonstrated by comparing the history-matching results to another LGR-based model. In the second case, we include a set of natural fractures in the same reservoir model and repeat history matching.

Embedded Discrete Fracture Model (EDFM)

As indicated earlier, discrete fracture modeling (DFM) is by far the most accurate method to simulate fluid flow in fractured reservoirs. This approach has not been widely utilized for field-scale applications. The large accuracy that DFM provides typically comes at a large computational cost. Handling discrete reservoir elements often requires some sort of unstructured gridding e.g., perpendicular bisector (PEBI) gridding. Not only laborious, such meshing techniques are also quite inflexible. This disadvantage severely limits further applications such as uncertainty and history-matching studies.

EDFM discretely describes fractures while maintaining an orthogonal structured grid. EDFM treatment is similar, in concept, to dual-continuum methods. This treatment portrays each control volume, defined by the intersection of a fracture with a gridblock, as a new fracture cell. The fracture cell will then connect to the cells corresponding to intersecting matrix and fractures through non-neighboring connections (NNCs). These NNCs are created such that the simulator can account for three new fluid-flow interfaces: between matrix and fracture segment; between two intersecting fracture segments; and between two segments of an individual fracture. Otherwise stated, the EDFM system allows fractures to be integrated in a virtual-like manner in any fashion/location within the reservoir model, which is why the parameterization of this system becomes useful.

New cells designated for fractures and their accompanying connections are added in the computation domain. This is visually illustrated in Fig. 1. Such arrangement enables flow interactions between cells that are not necessarily connected in the physical domain while maintaining a structured grid. Note that, in addition to the NNCs discussed above, flow between a fracture and an intersecting well is described by an effective well index that resembles Peaceman's work (1978). The calculated connection factors and indices only depend on the geometry and conductivity of rock matrix and fractures. In other words, the NNCs are phase and component independent, allowing EDFM to be a non-intrusive method that can be implemented in any connection-based, finite-difference reservoir simulator.

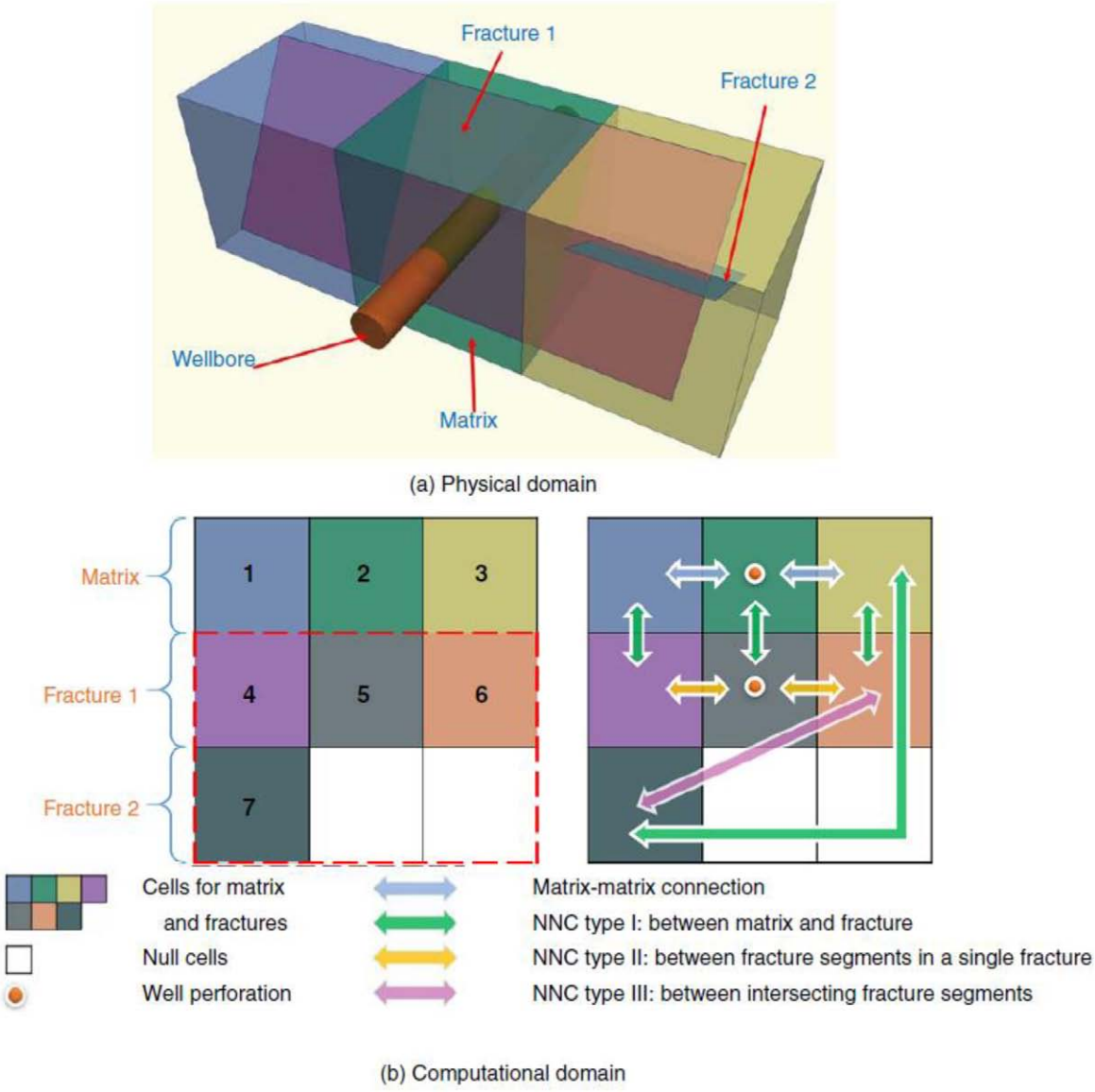

Figure 1—Illustration of cells and connections made in EDFM: (a) a case of 3 gridblocks that include a wellblock and 2 intersecting fractures, and (b) the corresponding cells and connections established in the computational domain (After Xu et al., 2017a).

Characterizing the dynamic behavior of natural fractures and hydraulically induced fractures is a critical component when optimizing well development, such as when analyzing well communication, optimal well/cluster spacing, or the impacts of the existing fracture framework. For this reason, EDFM is utilized for its proven ability to efficiently describe fluid flow and clearly indicate reserve distribution in unconventional reservoirs where these variable fracture conditions exist.

Natural Fractures in Unconventional Reservoirs

Natural Fractures has been thought of to play an important role in production from shale reservoirs. Production has been historically larger than the expectations (Gale et al. 2014). However, it is not yet fully understood how existing natural fracture networks contribute to overall permeability of the shale reservoir after a hydraulic-fracture treatment. Recent work suggests creation of a link with natural-fracture systems, which increases the effective surface area available to wellbore. The increased surface area will increase linear flow, the dominant flow regime (Gale et al. 2014). Although several studies have been published as

well as models have been developed to account for these interactions, a full quantitative model describing the contributions of the natural fractures in shale plays has not yet been established.

Information about the fractures that naturally occur near the producing reservoir is difficult to obtain. Techniques, such as microseismic imaging and imaging logs, can be practical for detecting natural fractures in the subsurface (Gale et al. 2014). However, much of this data is not available for many wells because microseismic imaging is expensive to run, may be poor in resolution, and/or has uncertainty in processing. Well-testing analysis is rarely conducted in shale gas wells because it typically requires shutting in the well for a long time. In the lack of direct data, most of the characterization work relied on examinations of core plugs and outcrops. While they give us valuable insight, they may, in many cases, be misleading (Gale et al. 2014). As being retrieved from the subsurface, the core undergoes secondary fractures due to stresses and changes in pressure. Therefore, it becomes difficult to distinguish natural fractures from core partings.

Outcrops are the only source that provides us with effective measurements of the lengths and orientation of the fractures. We may interpret this information as an analog for the undersurface. However, shale rock usually undergoes weathering and therefore shale outcrops are not as common as other sedimentary rocks (Gale et al. 2014). While these outcrops can represent the deep reservoir, they can sometimes give a misleading interpretation. Outcrops are subject to weathering and precipitation of minerals that do not necessarily occur in the subsurface.

If sufficient characterization of natural fractures is available, one may use a method proposed by Shakiba and Sepehrnoori (2015) to construct a realistic discrete fracture network (DFN) from the recorded microseismic events. The produced DFN are then incorporated in an EDFM grid as described before.

As characterization of natural fractures remains a challenge, EDFM reservoir simulations can still assist in locating and describing natural fractures. We can investigate different natural-fracture scenarios. For each scenario, multiple simulations may be run and stacked up against production history. By comparing results, we cannot fully characterize the natural-fracture network, but we can favor one scenario over another. Regardless of our certainty of the fracture network, EDFM simulations may provide insights about the contribution of natural fractures in hydrocarbon production from unconventional reservoirs. Moreover, we can assess the effect of natural fractures on characterization of other reservoir properties. This is investigated later in the paper by introducing random natural-fracture distribution in the near-well-bore volume.

History-Matching and Optimization Workflow

The integration of EDFM with available commercial simulators was made possible because EDFM calculations run in an external environment independent of the simulator's source code. With that said, further integration of EDFM into optimization and probabilistic forecasting tools has not been previously achieved. To achieve this, the pre-run EDFM calculations must be controlled and run in an automatic manner while the optimizer is re-arranging parameters.

In this paper, we are particularly interested in automatically matching production-history data while simultaneously integrating full parameterization of EDFM fractures (and their respective features), which can dominate model results. The algorithm steps for our general-purpose optimization workflow are shown in Fig. 2. In the first step, we parameterize general fracture attributes such as fracture half-length, height, aperture, and conductivity. Additional parameters can also include other reservoir properties, such as matrix permeability, relative permeability, and initial saturation. Other configurations, created by varying cluster spacing or frequency, can be exploited by the same method but are not shown here. All these parameters are defined on an optimizer; if a parameter is identified as uncertain, then it can be activated to vary either between categories or within number ranges based on prior assessment. Essentially, this method allows for full parameterization and sensitivity analysis of all known and unknown fracture characteristics to enhance the simulation runs to deliver more representative reservoir results.

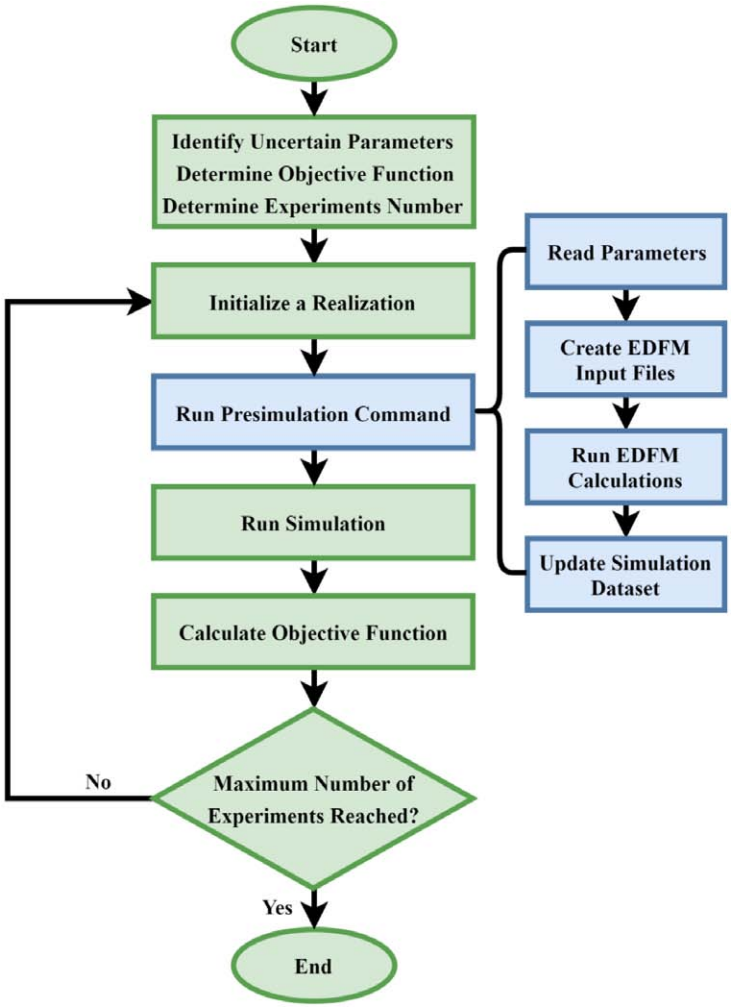

Figure 2—Flowchart of the proposed history matching and optimization method.

In the next step, parameters generated by the optimizer are exported to an external environment. Then, our presimulation command starts running in the background; it interprets parameters and generates an EDFM input accordingly. Then the code starts up EDFM calculations, upon which it updates the simulation dataset with the new non-neighboring blocks and their associated connections. The updated dataset is run on a simulator, and the objective function is calculated (Note: in this example, we are interested in minimizing history matching error).

The history-matching error is calculated in a way that reflects data significance and quality; and normalizes the error to the scale of data-points magnitude. The error Q_i is averaged from different data types for each well and is reported as a percentage according to the following equation (CMG-CMOST 2017):

$$Q_i = \frac{1}{\sum_{j=1}^{N(i)} tw_{i,j}} \times \sum_{j=1}^{N(i)} \frac{\sqrt{\frac{\sum_{t=1}^{T(i,j)} \left(mw_{i,j,t}^{m}\right)^2 \left(Y_{i,j,t}^{s} - Y_{i,j,t}^{m}\right)^2}{\sum_{t=1}^{T(i,j)} \left(mw_{i,j,t}^{m}\right)^2}}{Scale_{i,j}} \times 100\% \times tw_{i,j}$$

where *i, j, t* subscripts denote well, production data type, and time respectively. *N(i)* is the total number of production data types for well *i*. *T(i,j)* is the total number of measured data points for a data type *j*. *tw* and *mw* are the term weight for production data type, and for each measured data point respectively. Y^s and Y^m are simulation output- and measured-data points respectively.

In this study, we select an iterative optimizer that runs in cycles to search for history-matching solutions. Each cycle consists of two stages: a designed-exploration stage and a controlled-evolution stage (CMG-CMOST 2017). In the first stage, experimental design and Tabu search techniques are applied to carefully design an exploratory set of simulation dataset. This preliminary set allows us to gather as much information as possible about the solution space. In the second stage, the optimization algorithm statistically analyzes the results and excludes the values of parameters that result in divergence. This narrows down the search space for the next exploration stage. The algorithm routinely checks the rejected values to avoid getting trapped in local minima. This method allows early sampling of the full range of possible results/outcomes and then converges toward the defined goal, which in this case, is to reduce the history match error.

The workflow runs simulation experiments in series because the optimization algorithm learns and adapts from each simulation output. Hence, computation time required for the whole workflow to complete is dependent on simulation- and EDFM processing-run times, i.e., $t_{study} \approx n_{experiments}\ (t_{sim} + t_{EDFM})$. t_{study} is the computation time for the whole study; $n_{experiments}$ is the maximum number of experiments arbitrarily assigned by the user; and t_{sim} and t_{EDFM} are the run times for the simulation and EDFM preprocessor respectively.

Field Application in the Bakken

We test our history-matching workflow on a single horizontal well drilled in the Middle Bakken formation. The numerical-model configuration is adopted from Wantawin et al. (2017). Table 1 summarizes the properties of the reservoir model used in the study. We use a black-oil simulator in this example. Fracture clusters in a single stage are represented by multiple effective planar fractures and then integrated discretely using EDFM. In all simulations presented in the paper, we use two effective fractures per stage.

Table 1—Reservoir and fracture parameters for the simulation setup

Parameter	Value	Unit
Model dimensions (x × y × z)	10502 × 2640 × 50	ft
Number of gridblocks (x × y × z)	178 × 43 × 1	-
Initial reservoir pressure	7800 psi	psi
Reservoir temperature	245	°F
Total Compressibility	1×10^{-6}	psi^{-1}
Bubblepoint pressure	2500	psi
Oil density	50.86	lbm/ft^3
Gas density	0.92	-
Matrix porosity	0.056	-
Horizontal well length	8828	ft
Number of stages	15	-
Cluster spacing	118	ft
Fracture width	0.01	ft

We investigate uncertain parameters for two main scenarios: one incorporating only hydraulic fractures intersecting matrix cells and another incorporating both discrete hydraulic and natural fractures (Fig. 3). Table 2 lists the assessed range for four parameters we vary for both scenarios that we are most uncertain about. Note the following flexibility in fracture properties introduced by EDFM: fracture height may now be added as a variable regardless of layer thickness (layer thickness remains constant for all simulations), and fracture half-length is now independent of grid size and may vary continuously rather than discretely. Prior-probability distributions for all uncertain parameters are assumed uniform because information about

the distribution is not available. However, probability distributions, such as triangular and normal, could be applied in future implementations.

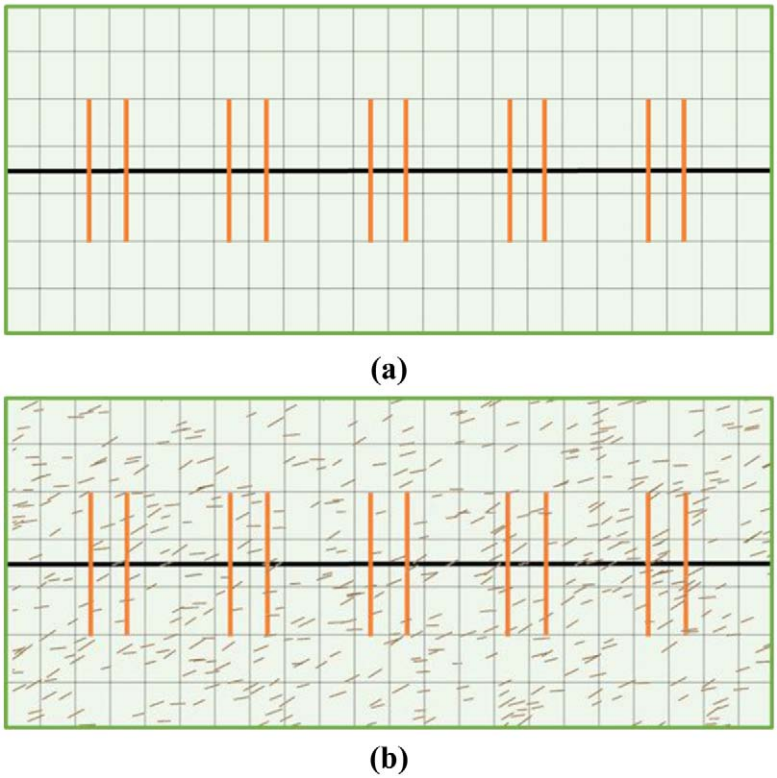

Figure 3—Schematic showing a plan view of the two modeling scenarios considered: (a) hydraulic fractures only; and (b) hydraulic and natural fractures. The horizontal well is represented by the solid black line, whereas hydraulic fractures are represented by the perpendicular orange lines. Natural fractures are randomly distributed in the subsurface.

Table 2—Predefined ranges for the uncertain parameters

Uncertain parameter	Unit	Type	Base Case	Minimum	Maximum
Matrix permeability	*μd*	Continuous	49.42	1	50
Fracture conductivity	md-ft	Continuous	500	5	500
Fracture half length	ft	Continuous	92.1	90	400
Fracture height	ft	Continuous	50	20	50

We omit uncertainty for parameters that were previously recognized uncertain, such as initial water saturation, wettability, and effective-fracture quantity. Based on the findings from Wantawin et al. (2017a), we assume an initial water saturation of 50% and oil-wet rock with the relative permeability curve shown in Fig. 4. Capillary-induced flow-drive forces are trivial here; thus, we do not account for capillary pressure data.

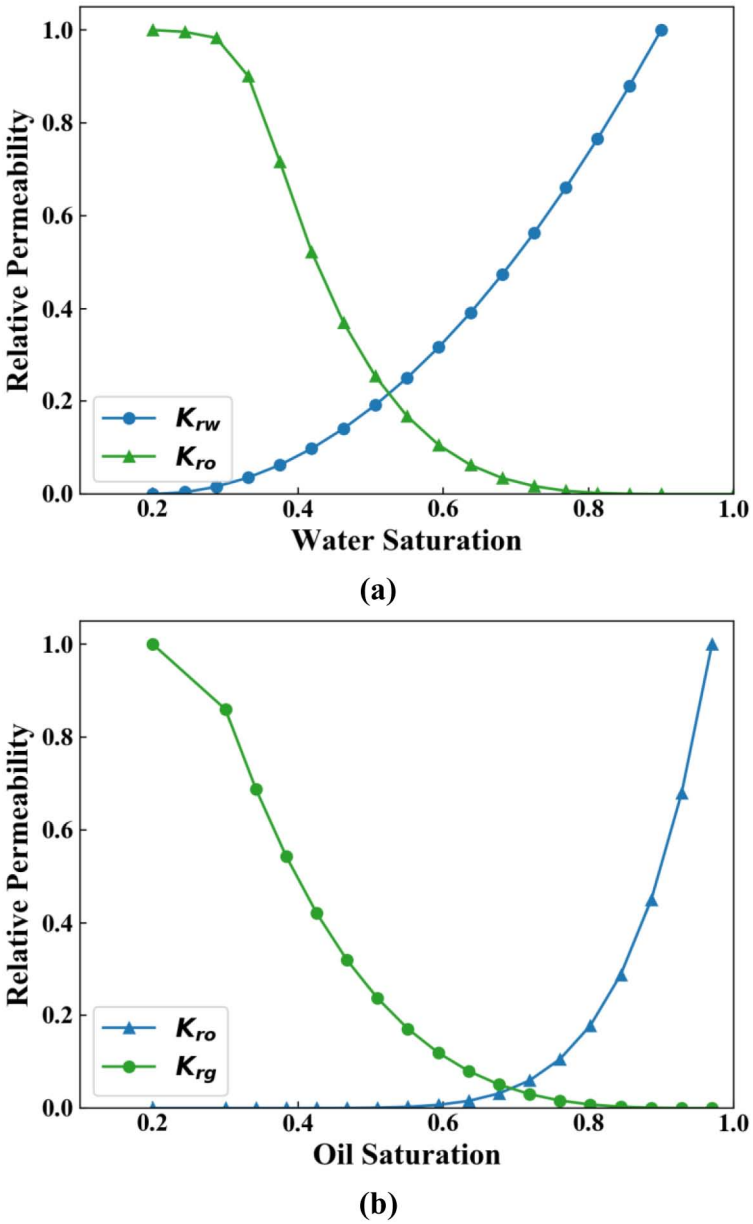

Figure 4—Relative permeability curves for the oil-wet rock adopted in the reservoir (from Wantawin et al. 2017a).

In the second scenario, we surround the wellbore with natural fractures using the optimal realization, obtained from history matching the first scenario as a base case. An ensemble of 1000 natural fractures are randomly scattered in the subsurface. Connections between natural fractures and the well are deactivated because the horizontal lateral is cased and cemented. Each natural fracture has 100-ft length, 0.001-ft width, and 3000-md permeability. We assume vertically dipping fractures that cut across the whole reservoir thickness (50 ft).

Varying natural-fracture locations and properties are not considered here because we are interested in the effect of natural-fracture presence on the characterization of induced-fracture network. However, we can address natural-fracture uncertainty in future work once we become certain enough about other subsurface and completion properties.

For each scenario, we are interested in obtaining realizations that satisfy a history-matching criterion; the cases yielding a history-matching error smaller than 5% are accepted as possible solutions. Oil-production data are set as constraints for simulation over the recorded period, and history-matching error is calculated

based on the bottom-hole pressure (BHP) and gas-production rate data. Each data type is equally weighted for the purpose of error calculations yielding an objective function we refer to as the global history-matching error. Water-production rates were not reported and were assumed to be 25% of oil production rates.

Results and Discussion

For the first scenario, after running 500 simulation experiments, the workflow generated 412 realizations qualifying as solutions. Moreover, the global error for the optimal case was 4.15% (Fig. 5). This error is significantly smaller than that for the base case (5.15%) which is based on previously published history-matching results (Wantawin et al. 2017a). The parameters for the optimal case are: 0.0375 md for matrix permeability; 448 md-ft for hydraulic-fractures conductivities; 155.1 ft for fracture half length; and 35 ft for fracture height.

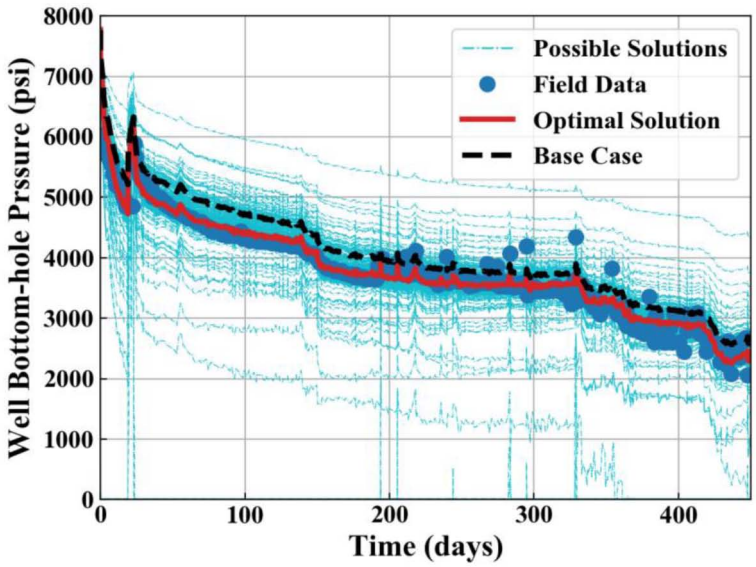

(a)

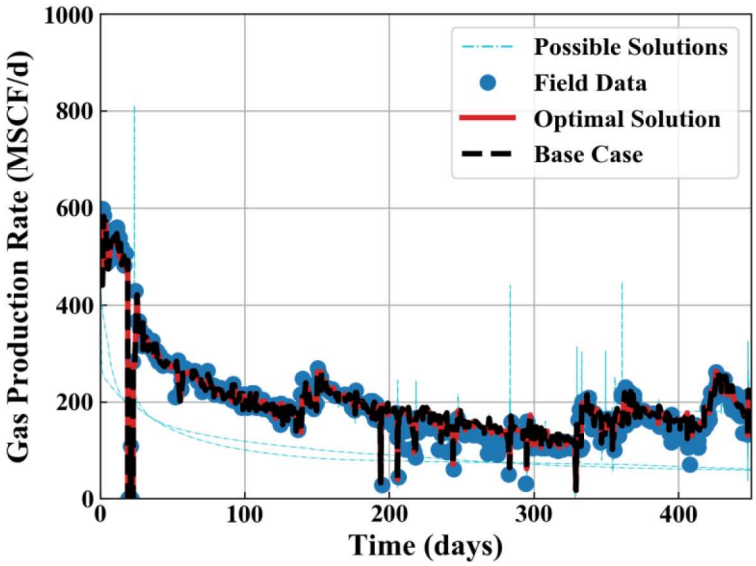

(b)

Figure 5—History-matching results for scenario 1. (a) BHP response for base case, general solutions and optimal solution; and (b) gas-production-rate responses. Parameters for the base case are listed in Table 2.

We affiliate this significant improvement in history-matching quality with the added capability of varying fracture dimensions on a continuous level rather than discrete, which was previously limited by the basic gridblock dimensions of LGR models. This flexibility also resulted in generating realizations that more closely match our expectations and reported data for the Middle Bakken (Nojabaei et al. 2013; Cherian et al. 2013).

Next, we include natural fractures in the optimal solution obtained from the previous step and we repeat history matching. A 3D construction of one subsurface realization is displayed in Fig. 6. In this second scenario, the global error reduced further from 4.94%, for the base case, to 4.12%, for the optimal solution. For the optimal realization, matrix permeability decreased to 0.0332 md. Hydraulic-fracture conductivity contracted to 266 md-ft; its half-length slightly increased to 161.5 ft; and its height shrank to 31.5 ft.

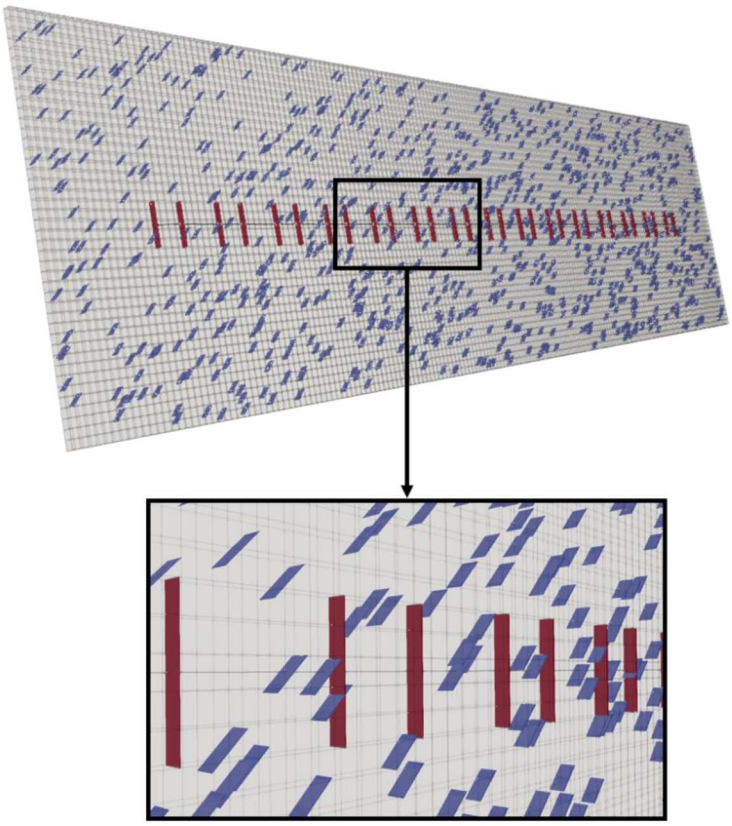

Figure 6—3D visualization of the grid for one of the history-matching realizations for the second scenario. Dark red represents EDFM hydraulic fractures, whereas blue represents EDFM natural fractures. Picture is drawn to scale.

Fig. 7 compares the posteriori frequency for uncertain parameters between the two scenarios. After adding natural fractures to the subsurface, matrix-permeability distribution slightly shifts towards decreasing permeability on a logarithmic scale. This observation is consistent with our expectation; natural fractures act as fluid pathways from the matrix to the effective wellbore. The presence of natural fractures must be subsidized by decrease in matrix permeability to deliver the same amount of fluid. In addition, the narrow distribution suggests that the history-matching-error response is highly sensitive on matrix permeability; and there is probably distinctive small region of matrix permeability for accepted realizations (here it ranges from 0.0303 to 0.0367 md for the 2nd scenario).

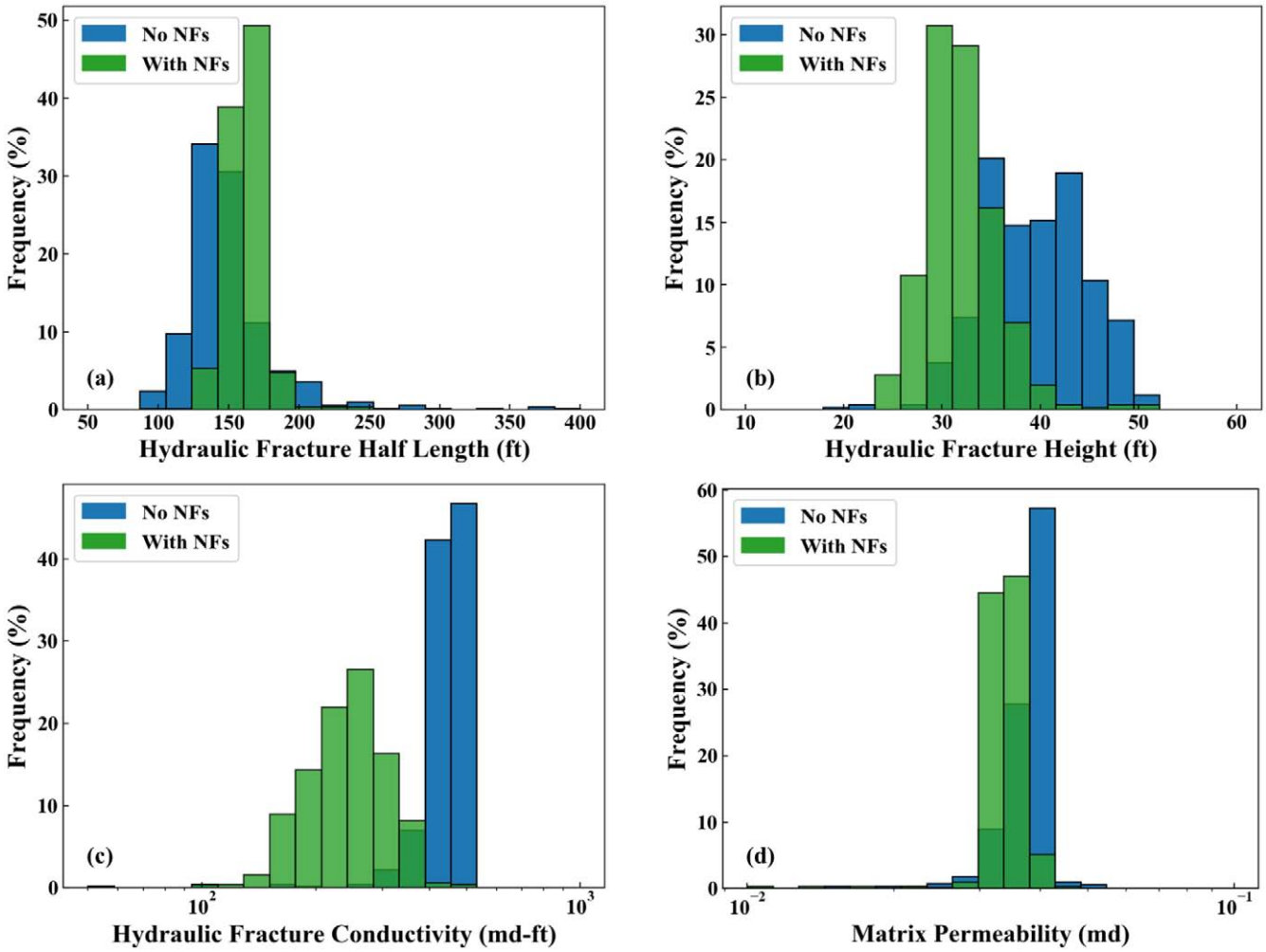

Figure 7—Histograms showing the posterior distribution of uncertain parameters. The data are collected from all the general realizations exploited after history matching of the two scenarios.

Conductivity of induced fractures follow the same trend of reduction that counterbalances the natural fractures influence. However, the conductivity distribution has larger dispersion suggesting smaller sensitivity. Here, the fracture conductivity varies from 149.0 to 387.5 md-ft for accepted realizations. The conductivity distribution exhibits smaller deviation for the second scenario. This can be explained by an argument that the upper bound of uncertainty range might have been underestimated (as evident in Fig. 7.c).

Although we expected hydraulic fractures to shrink in length in response to natural fractures, results demonstrate the opposite. Fracture half-length spans from 142.0 to 179.5 ft for accepted realizations. The increase in half-length means more direct connections between hydraulic and natural fractures (see Fig. 6); and that could be the reason behind the observed lengthening. This lengthening in half-length is offset by a notable decrease in fracture height (as shown in Fig. 7.b). Fracture height's posterior distribution is less uniform in the case of natural fractures, suggesting that it has larger effect to the response when natural fractures are added to the model.

We show a comparison between the grid pressures for the two scenarios (Fig. 8). Notice how the pressure profile becomes non-uniform in the presence of natural fractures. There appears to be regions of increased pressure depletion around natural-fracture clusters. This implies that the distribution of natural fractures in the reservoir is crucial for simulation results.

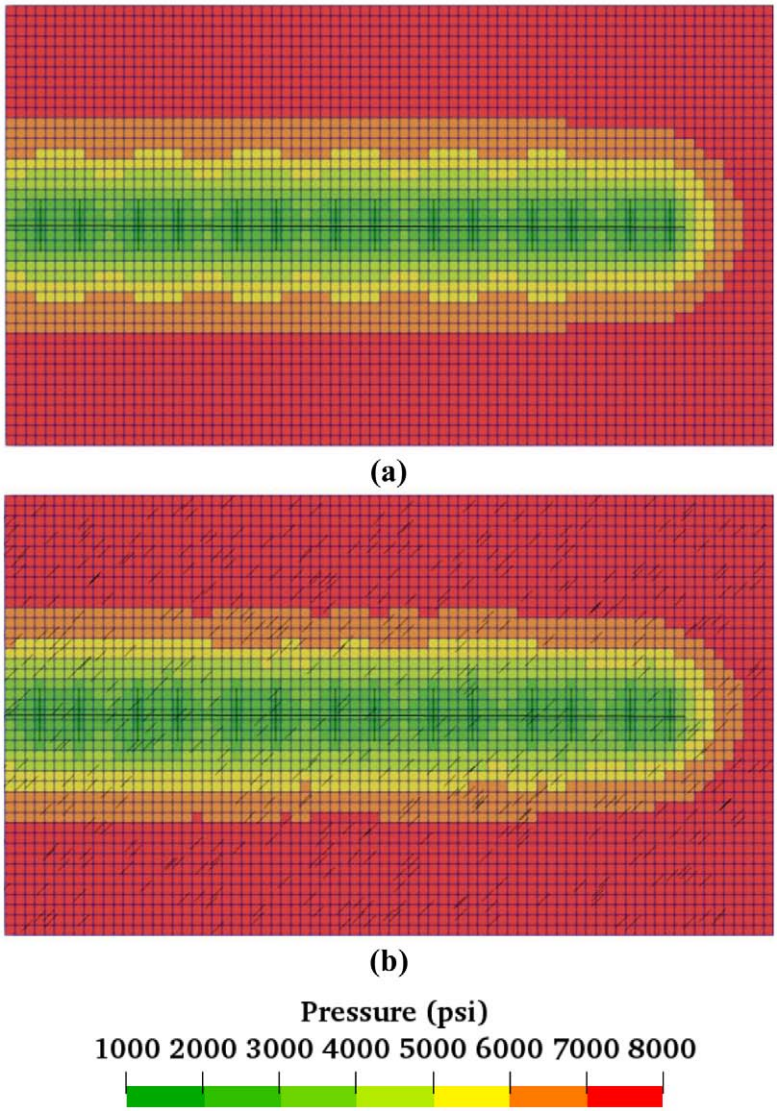

Figure 8—Pressure profiles after five months of production for the optimal cases of (a) the first scenario, and (b) the second scenario. Gridblocks i = 92–170, j = 1–43 and k=1 are displayed in both figures. The long horizontal line in the middle represents the well and the black lines that intersect with the mesh represent fractures.

As demonstrated earlier, this method can be applied for uncertainty and optimization problems beyond history matching. Here, we conduct a simple one-factor-at-a-time (OFAAT) sensitivity study for uncertain parameters on the second scenario. Although we believe that the uncertain parameters are not independent and their combined effects on the objective function are strong and cannot be neglected, an OFAAT analysis still provides valuable insight on single effects (Fig. 9). Results from this analysis are consistent with the findings we infer from the posterior parameter distributions.

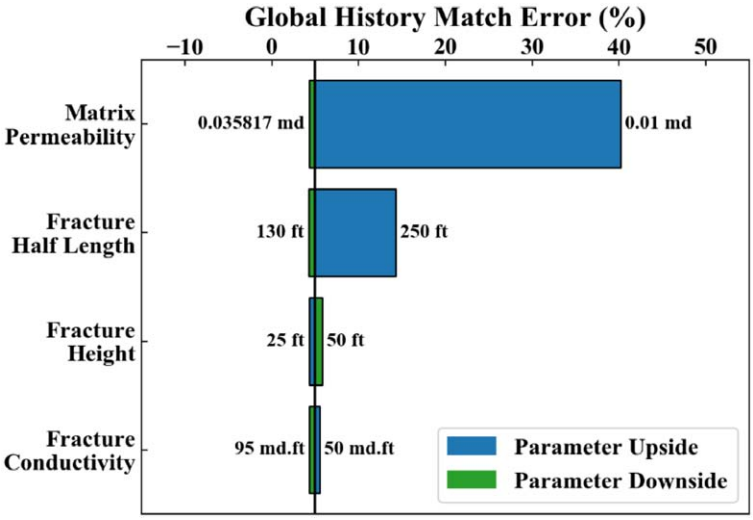

Figure 9—OFAAT sensitivity analysis for the second scenario. Ranges for uncertain parameters are the same as Table 2.

We extend production for the accepted realizations for both scenarios to make future production forecasts and estimate EUR. After history period, production from the well is controlled by constraints of 500-psi minimum BHP and 250 STB maximum oil production rate. Whereas solutions' responses exhibit unnoticeable variation during history period, they undergo significant divergence afterwards (Fig. 10). EUR is assessed by calculating cumulative oil production of the well for an assumed, prolonged lifetime of 30 years. P10, P50, and P90 of EUR for the first scenario are 538.06 MSTB, 547.21 MSTB, and 553.44 MSTB, respectively. In this study, we define P10 as the low estimate (i.e., 90% of the estimates are larger than P10).

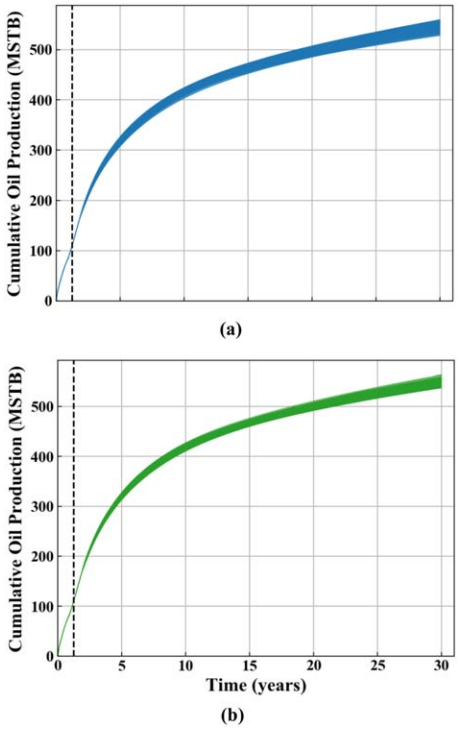

Figure 10—Oil cumulative-production forecast for 30 years based on accepted history-matching solutions for: (a) 412 accepted realizations with the first configuration (no natural fractures); and (b) 451 accepted realizations with the second configuration (with natural fractures). The dashed line represents the end of field-recorded period.

We notice a decrease in recovery for the new solutions compared to the figures reported by the study mentioned earlier. This decline can be explained by the significant decrease in matrix permeability for the realizations. We report about 15 MSTB variation between the P10 and P90 estimates, whereas the variation was reported to be about 41 MSTB for the previous study (Wantawin et al. 2017a). Our method generated more solutions that satisfy the acceptance criterion, but we must be careful about this comparison because the number of uncertain parameters is smaller here.

Li et al. (2011) demonstrated that various configurations could produce the same production history; and that a quality match of production profiles does not guarantee reliable reserve estimation. P10, P50, and P90 of EUR for the second scenario are 541.41 MSTB, 546.78 MSTB, and 553.93 MSTB, respectively. The confidence interval of EUR is slightly wider for the first scenario (Fig. 11). However, the difference between the P50 of the two cases is insignificant (less than 1%). Even though adding natural fractures to the subsurface significantly alters the history-matching realizations (as illustrated earlier), the estimated EUR appears to remain similar.

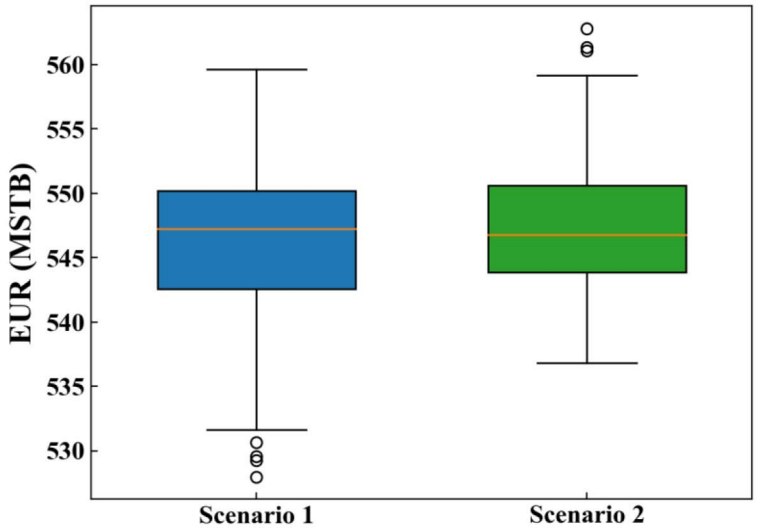

Figure 11—Boxplots of the EUR for accepted realizations for the two scenarios.

Although we only take in account cumulative-oil production for EUR estimates, we report similarity between predicted cumulative-gas production for the two ensembles (Fig. 12). The agreement between prediction outcomes informs us that using matrix blocks with an effective permeability leads to similar end results as using blocks with detailed description of natural fractures. For the case considered here, we find support that justifies the selection of a simple (effective permeability) model as an analog of the complex-fracture network. However, it will remain for future work to investigate the comparability for different natural-fracture scenarios and reservoir properties.

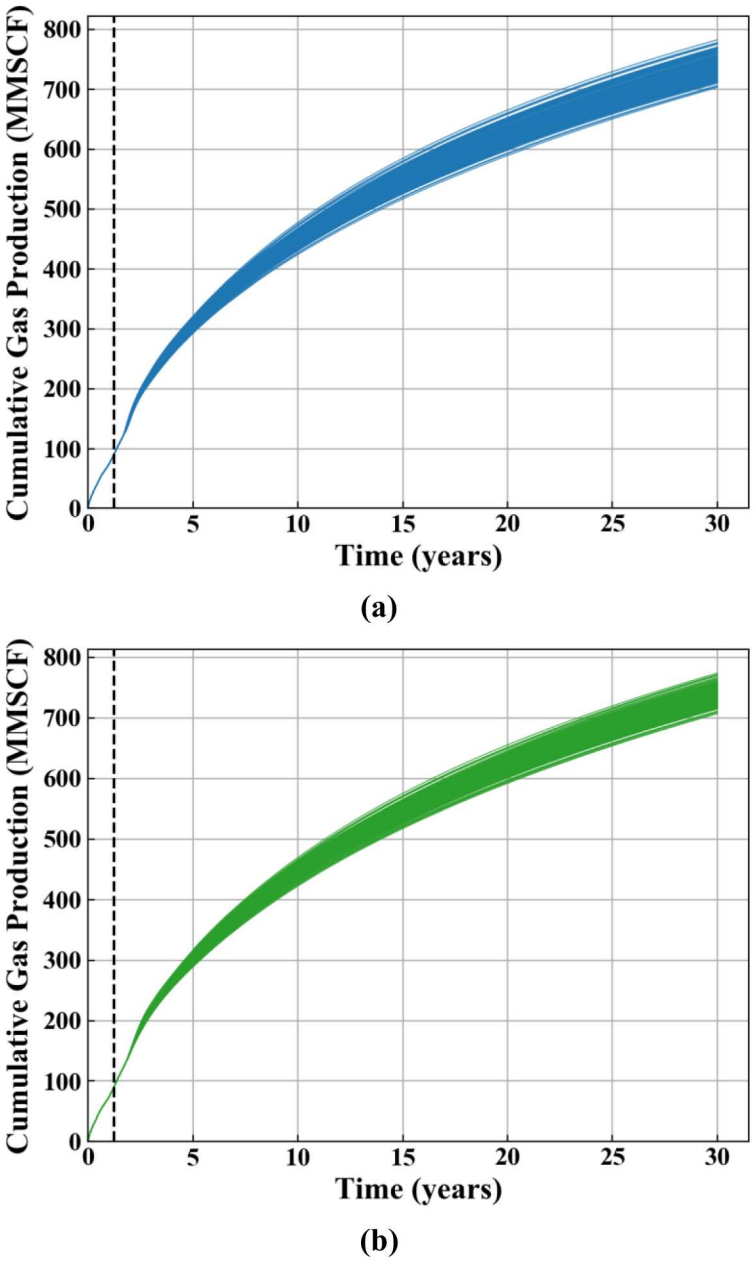

Figure 12—Gas cumulative-production forecast for 30 years based on accepted history-matching solutions for: (a) first scenario; and (b) second scenario.

In this study, we illustrated the efficiency of our workflow to assist find history-matching solutions when uncertainty is large and multi-dimensional. We only applied it, however, to the Bakken tight-oil play that has permeability significantly larger than many active shale plays. Further investigation should be focused on applying the workflow on cases from smaller permeability shales and testing the integrity of simple bi-wing planar-fractures models.

Conclusions

We emphasize the importance of computer-assisted history-matching methods to address the multi-variable uncertainty that are frequently encountered in unconventional reservoirs. After applying our automated history-matching method to a horizontal well in the Middle Bakken formation, along with taking natural fractures into account, we conclude:

- Integrating EDFM fractures into the automated history-matching workflow adds the advantage of easily adjustable fracture geometry. These new capabilities contribute to reducing the achievable history-matching error and allow for more advanced reservoir characterization.
- Matrix permeability followed by fracture half-length have the most significant effect on the history-matching error. The parameter distribution for accepted realizations have larger dispersion for fracture conductivity and height.
- Adding an EDFM natural-fracture set to the subsurface (in our case) has the following effects on parameters posterior distribution: matrix permeability recedes to smaller values; hydraulic-fracture height and conductivity shrinks; and hydraulic fractures extend to longer half lengths.
- Accepted realizations from the first and second scenarios (with or without natural fractures) bring about roughly the same projected EUR. Therefore, for the case considered here, effective matrix permeability (that replaces natural fractures) is proven adequate to represent the subsurface.

By applying this method, we retrieve an ensemble of solutions rather than a single solution. Estimation of EUR can be probabilistically assessed from future projections of the retrieved solutions. The method is computationally robust and easily adaptable to different scenarios, and it can be extended to subsequent optimization for unconventional-resources development.

Acknowledgements

The authors would like to acknowledge Computer Modeling Group Ltd. for providing CMG simulation package and SimTech LLC for providing EDFM software for this study. We also thank Fabio Bordeaux Rego for his support.

References

Cherian, B.V, Nichols, C.M., Panjaitan, M.L., Nochols, C.M., and Krishnamurthy, J.K. 2013. Asset Development Drivers in the Bakken and Three Forks. Paper SPE 163855, presented at the SPE Hydraulic Fracturing Technology Conference, The Woodlands, Texas, 4-6 February.

Cipolla, C.L., Lolon, E.P., Erdle, J.C., and Rubin, B. 2010. Reservoir Modeling in Shale-Gas Reservoirs. *SPE Reservoir Evaluation & Engineering* **13** (4): 638–653.

CMG, 2017. *CMOST User's Guide*, Computer Modeling Group Ltd.

Dachanuwattana, S., Jin, J., Zuloaga-Molero, P., Li, X., Xu, Y., Sepehrnoori, K., Yu, W., and Miao, J. 2018b. Application of Proxy-based MCMC and EDFM to History Match a Vaca Muerta Shale Oil Well. *Fuel* **220**: 490–502.

Dachanuwattana, S., Xia, Z., Yu, W., Qu, L., Wang, P., Liu, W., Miao, J., and Sepehrnoori, K. 2018a. Application of Proxy-based MCMC and EDFM to History Match a Shale Gas Condensate Well. *Journal of Petroleum Science and Engineering* **167**: 486–497.

Ding, Y., Basquet, R., and Bourbiaux, B. 2006. Upscaling Fracture Networks for Simulation of Horizontal Wells Using a Dual-Porosity Reservoir Simulator. *SPE Reservoir Evaluation & Engineering* **9** (5): 513–520.

Du, C., Zhang, X., Zhan, L., Gu, H., Hay, B., Tushingham, K., and Ma, Y.Z. 2010. Modeling Hydraulic Fracturing Induced Fracture Networks in Shale Gas Reservoirs as a Dual Porosity System. Paper SPE 132180, presented at the CPS/SPE International Oil & Gas Conference and Exhibition, Beijing, China, 8-10 June.

Gale, J.F., Laubach, S.E., Olson, J.E., Eichhubl, P., and Fall, A. 2014. Natural Fractures in Shale: A Review and New Observations. *AAPG Bulletin* **98** (11): 2165–2216.

Gong, B., Karimi-Fard, M., and Durlofsky, L.J. 2008. Upscaling Discrete Fracture Characterizations to Dual-Porosity, Dual-Permeability Models for Efficient Simulation of Flow with Strong Gravitational Effects. *SPE Journal* **13** (1): 58–67.

Kazemi, H., Merrill, L.S., Porterfield, K.L., and Zeman, P.R. 1976. Numerical Simulation of Water-Oil Flow in Naturally Fractured Reservoirs. *SPE Journal* **16** (6): 317–326.

Li, J., Du, C., and Zhang, X. 2011. Critical Evaluation of Shale Gas Reservoir Simulation Approaches: Single-Porosity and Dual-Porosity Modeling. Paper SPE 141756, presented at the SPE Middle East Unconventional Gas Conference and Exhibition, San Antonio, Texas, 31 January-2 February.

Luo, S., Wolff, M., Ciosek, J., Rasdi, M.F., Neal, L., Arulampalam, P., and Willis, S.K. 2011. Probabilistic Reservoir Simulation Workflow for Unconventional Resource Play: Bakken Case Study. Paper SPE 142896, presented at the SPE EUROPEC/EAGE Annual Conference and Exhibition, Vienna, Austria, 23-26 May.

Moinfar, A., Narr, W., Hui, M.H., Mallison, B.T., and Lee, S.H. 2011. Comparison of Discrete-Fracture and Dual-Permeability Models for Multiphase Flow in Naturally Fractured Reservoirs. Paper SPE 142295, presented at the SPE Reservoir Simulation Symposium, The Woodlands, Texas, USA, 21-23 February.

Moinfar, A., Varavei, A., Sepehrnoori, K., and Johns, R. 2014. Development of an Efficient Embedded Discrete Fracture Model for 3D Compositional Reservoir Simulation in Fractured Reservoirs. *SPE Journal* **19** (2): 289–303.

Nojabaei, B., Jhons R.T., and Chu, L. 2013. Effect of Capillary Pressure on Phase Behavior in Tight Rocks and Shales. *SPE Reservoir Evaluation & Engineering* **16** (3): 281–289.

Rossen, R.H. 1977. Simulation of Naturally Fractured Reservoirs with Semi-Implicit Source Terms. *SPE Journal* **17** (3): 201–210.

Shakiba, M., de Araujo Cavalcante Filho, J.S., and Sepehrnoori, K. 2018. Using Embedded Discrete Fracture Model (EDFM) in Numerical Simulation of Complex Hydraulic Fracture Networks Calibrated by Microseismic Monitoring Data. *Journal of Natural Gas Science and Engineering* **55**: 495–507.

Sun, H., Chawathe, A., Hoteit, H., Shi, X., and Li, L. 2015. Understanding Shale Gas Flow Behavior Using Numerical Simulation. *SPE Journal* **20** (1): 142–154.

Tripoppoom, S., Yu, W., Huang, H., Sepehrnoori, K., Song, W., Dachanuwattana, S. 2019. A Practical and Efficient Iterative History Matching Workflow for Shale Gas Well Coupling Multiple Objective Functions, Multiple Proxy-based MCMC and EDFM. *Journal of Petroleum Science and Engineering* **176**: 594–611.

Wantawin, M., Yu, W., and Sepehrnoori, K. 2017a. An Iterative Work Flow for History Matching by Use of Design of Experiment, Response-Surface Methodology, and Markov Chain Monte Carlo Algorithm Applied to Tight Oil Reservoirs. *SPE Reservoir Evaluation & Engineering* **20** (3): 613–626.

Wantawin, M., Yu, W., Dachanuwattana, S., and Sepehrnoori, K. 2017b. An Iterative Response-Surface Methodology by Use of High-Degree-Polynomial Proxy Models for Integrated History Matching and Probabilistic Forecasting Applied to Shale-Gas Reservoirs. *SPE Journal* **22** (6): 2012–2031.

Xu, Y., Cavalcante Filho, J.S.A., Yu, W., and Sepehrnoori, K. 2017a. Discrete-Fracture Modeling of Complex Hydraulic-Fracture Geometries in Reservoir Simulators. *SPE Reservoir Evaluation & Engineering* **20** (2): 403–422.

Xu, Y., Yu, W., and Sepehrnoori, K. 2017b. Modeling Dynamic Behaviors of Complex Fractures in Conventional Reservoir Simulators. Paper URTeC 2670513, presented at the SPE/AAPG/SEG Unconventional Resources Technology Conference, Austin, Texas, 24-26 July.

Xu, Y., Yu, W., Li, N., Lolon, E., and Sepehrnoori, K. 2018. Modeling Well Performance in Piceance Basin Niobrara Formation Using Embedded Discrete Fracture Model. Paper URTeC 2901327, presented at the SPE/AAPG/SEG Unconventional Resources Technology Conference, Houston, Texas, 23-25 July.

Yang, D., Xue, X., and Chen, J. 2018. High Resolution Hydraulic Fracture Network Modeling Using Flexible Dual Porosity Dual Permeability Framework. Paper SPE 190096, presented at the SPE Western Regional Meeting, Garden Grove, California, 22–26 April.

Yu, W., and Sepehrnoori, K. 2018. Shale Gas and Tight Oil Reservoir Simulation, 1st Ed.; Publisher: Elsevier, Cambridge, USA. ISBN: 978-0-12-813868-7.

Yu, W., Tripoppoom, S., Sepehrnoori, K., and Miao, J. 2018. An Automatic History-Matching Workflow for Unconventional Reservoirs Coupling MCMC and Non-Intrusive EDFM Methods. Paper SPE 191473, presented at the SPE Annual Technical Conference and Exhibition, Dallas, Texas, 24-26 September.